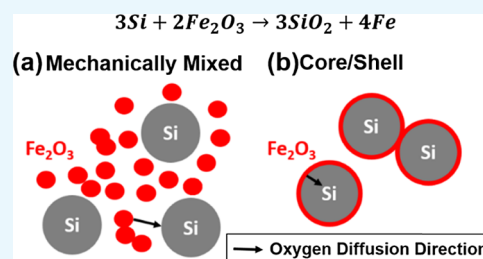# ACS OMEGA

Electroless Deposition and Ignition Properties of Si/Fe$_2$O$_3$ Core/Shell Nanothermites

Sidi Huang,[†,§] Sili Deng,[†,§] Yue Jiang,[‡] Jiheng Zhao,[†] and Xiaolin Zheng[*,†]

[†]Department of Mechanical Engineering and [‡]Department of Materials Science and Engineering, Stanford University, Stanford, California 94305, United States

ABSTRACT: Thermite, a composite of metal and metal oxide, finds wide applications in power and thermal generation systems that require high-energy density. Most of the researches on thermites have focused on using aluminum (Al) particles as the fuel. However, Al particles are sensitive to electrostatic discharge, friction, and mechanical impact, imposing a challenge for the safe handling and storage of Al-based thermites. Silicon (Si) is another attractive fuel for thermites because of its high-energy content, thin native oxide layer, and facile surface functionality. Several studies showed that the combustion properties of Si-based thermites are comparable to those of Al-based thermites. However, little is known about the ignition properties of Si-based thermites. In this work, we determined the reaction onset temperatures of mechanically mixed (MM) Si/Fe$_2$O$_3$ nanothermites and Si/Fe$_2$O$_3$ core/shell (CS) nanothermites using differential scanning calorimetry. The Si/Fe$_2$O$_3$ CS nanothermites were prepared by an electroless deposition method. We found that the Si/Fe$_2$O$_3$ CS nanoparticles (NPs) had a lower reaction onset temperature ($\sim$550 °C) than the MM Si/Fe$_2$O$_3$ nanothermites (>650 °C). The onset temperature of the Si/Fe$_2$O$_3$ CS nanothermites is also insensitive to the size of the Si core NP. These results indicate that the interfacial contact quality between Si and Fe$_2$O$_3$ is the dominant factor for determining the ignition properties of thermites. Finally, the reaction onset temperature of the Si/Fe$_2$O$_3$ CS NPs is comparable to that of the commonly used Al-based nanothermites, suggesting that Si is an attractive fuel for thermites.

$$3Si + 2Fe_2O_3 \rightarrow 3SiO_2 + 4Fe$$

(a) Mechanically Mixed (b) Core/Shell

→ Oxygen Diffusion Direction

INTRODUCTION

Thermite is an energetic composite of metals as fuels (e.g., Al, B, and Si) and metal oxides as oxidizers (e.g., CuO, Fe$_2$O$_3$, and WO$_3$). Once ignited, thermite releases a large amount of heat and thus finds applications, ranging from aerospace propulsion, thermal batteries, waste disposals, and power generation for microsystems to material synthesis.[1−4] Most of the researches on thermites have focused on using aluminum (Al) as the fuel.[5−11] However, Al, especially Al nanoparticles (Al NPs), is sensitive to electrostatic discharge, friction, and mechanical impact,[12] imposing a challenge for the safe handling and storage of Al-based thermites. In addition, Al particles have a native oxide layer of 2−6 nm, which acts as a dead mass.[13] Among other fuels such as red phosphorus[14] and boron,[15,16] silicon (Si) is another attractive fuel for thermites because it has high volumetric and specific energy densities (75.1 MJ/L and 32.2 MJ/kg, respectively) similar to those of Al (83.8 MJ/L and 31.0 MJ/kg, respectively). Si also has a thinner native oxide layer of 1−3 nm than Al,[17] and it is resistant to electrostatic discharge. Importantly, the surface of Si can be easily functionalized,[18,19] facilitating the use of coating and surface modification to tailor its ignition and burning properties. Several previous studies have shown that Si-based thermites have comparable combustion properties as Al-based thermites,[18,20,21] in terms of adiabatic combustion temperatures ($\sim$3000 K) and burning rates (40−530 m/s).[22] However, little is known about the ignition properties of Si-based thermites and their dependence on the structure of thermites.

Herein, we study the ignition properties, in terms of reaction onset temperatures, of Si and Fe$_2$O$_3$ thermite mixtures. The reason for choosing Fe$_2$O$_3$ as the oxidizer is that Al/Fe$_2$O$_3$ is one of the most studied thermite systems.[23] Moreover, the thermite reaction between Si and Fe$_2$O$_3$ ($3Si + 2Fe_2O_3 \rightarrow 3SiO_2 + 4Fe$, 12.9 MJ/kg of Si) has the least amount of gaseous byproducts among thermites,[20] allowing us to focus on the structural effect on the oxygen diffusion process that is critical to ignition. In particular, we compared the reaction onset temperatures of Si/Fe$_2$O$_3$ core/shell (CS) particles with those of the mechanically mixed (MM) Si/Fe$_2$O$_3$ powders (Figure 1). We found that the Si/Fe$_2$O$_3$ CS NPs had a lower reaction onset temperature ($\sim$550 °C) than the MM Si/Fe$_2$O$_3$ nanothermites (>650 °C). These results indicate that the interfacial contact quality between Si and Fe$_2$O$_3$ is the dominant factor for determining the ignition properties of thermites, a phenomenon similar to that in Al-based thermites.[3] Finally, the reaction onset temperature of the Si/Fe$_2$O$_3$ CS NPs is comparable to that of the commonly used Al-based nanothermites, suggesting that Si is an attractive fuel for thermites.

We investigated the ignition properties of Si/Fe$_2$O$_3$ nanothermites by using Si NPs of two different sizes (20−30 nm, US Research Nanomaterials, and 100 nm, Skyspring Nanomaterials Inc.). The oxygen content of these particles is summarized in Table 1. Overall, the oxygen content of both sizes of Si NPs is

$$3Si + 2Fe_2O_3 \rightarrow 3SiO_2 + 4Fe$$

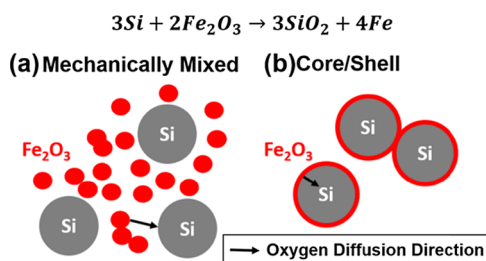**(a) Mechanically Mixed** **(b) Core/Shell**

Figure 1. Schematics of (a) MM and (b) CS Si/Fe$_2$O$_3$ thermites. The improved contact between Si and Fe$_2$O$_3$ in the CS structure facilitates the oxygen diffusion process and hence lowers the reaction onset temperature.

Table 1. Oxygen Contents of Different Si Particles

material	oxygen content (wt %)	references
20−30 nm Si	0.81	26
100 nm Si	0.50	27

negligible. The MM Si/Fe$_2$O$_3$ samples (Figure 1a) were prepared by dispersing 100 mg of Si and 380.2 mg of Fe$_2$O$_3$ into 10 mL of hexane, followed by sonication for 30 min and drying on a hot plate at 100 °C. The Si/Fe$_2$O$_3$ CS NPs (Figure 1b) were prepared by coating Si with an Fe$_2$O$_3$ shell using an electroless deposition method.[24] As schematically illustrated in Figure 2a, the Si particles were first coated with a Pd layer through electrostatic plating. Then, Pd was replaced by Fe through electroless plating. The formed Si/Fe NPs were converted to Si/Fe$_2$O$_3$ CS NPs by thermal annealing. The detailed synthesis process is described in the Methods section.

■ RESULTS AND DISCUSSION

The scanning electron microscopy (SEM) images in Figure 2b−e show the representative morphologies of the initial Si particles (Figure 2b,c, average diameter: 100 nm) and the final coated Si/Fe$_2$O$_3$ NPs (Figure 2d,e). The surface of the initial Si particles is smooth (Figure 2c), and it becomes rather rough after the synthesis (Figure 2e), indicating a successful coating. SEM inspection over a wide range of samples shows that the surface of the Si particle is coated with a shell. The coating of Fe$_2$O$_3$ over the Si surface is also confirmed by transmission electron microscopy (TEM) and energy-dispersive X-ray spectroscopy (EDXS) mapping. It should be noted that the SEM images were taken for the 100 nm Si NPs because of the spatial resolution limit and that the TEM images were taken for

20−30 nm Si particles for better electron transmission. Both the TEM and standing TEM (STEM) images (Figure 3a,b) suggest that the final particle has a CS structure. The EDXS element mapping of the boxed regime in Figure 3a shows the coexistence of strong Fe element and O element signals and relatively weak Si signals, indicating that a layer of Fe$_2$O$_3$ has been deposited on the surface of Si. However, because the initial sizes and shapes of Si particle have an inherent distribution, it is difficult to determine the exact thickness of iron oxide. Instead, we have estimated the Si/Fe$_2$O$_3$ equivalence ratios using an inductively coupled plasma optical emission spectroscopy (Thermo Scientific ICAP 6300 Duo view spectrometer) system. The estimated equivalence ratios of 20−30 nm and 100 nm Si/Fe$_2$O$_3$ CS particles are 24.1 ± 0.15 and 6.07 ± 0.02, respectively. In addition, the X-ray photoelectron spectroscopy (XPS) analysis of the Si/Fe$_2$O$_3$ CS NP in Figure 3f shows the characteristic iron oxide peaks (Fe 2p$_{3/2}$ and Fe 2p$_{1/2}$, 711.4 and 724.2 eV, respectively), confirming the shell chemical composition of Fe$_2$O$_3$. Finally, the X-ray diffraction (XRD) analysis of both the Si/Fe$_2$O$_3$ CS and MM NPs shows the characteristic peaks of Si and Fe$_2$O$_3$ (Figure 3g). The above characterizations indicate that we have synthesized Si/Fe$_2$O$_3$ CS NPs.

Next, we used differential scanning calorimetry (DSC) to determine the reaction onset temperatures of Si/Fe$_2$O$_3$ CS NPs and compare with those of the MM NPs. Figure 4 shows the representative baseline-corrected DSC profiles of Si/Fe$_2$O$_3$ CS and MM samples with two different sizes of the Si particle. First, the onset temperature of the Si/Fe$_2$O$_3$ CS NPs is about 550 °C, which is about 100−150 °C lower than that of the MM samples. This confirms that the CS structure has more facile oxygen diffusion process because of its better interfacial contact between Si and Fe$_2$O$_3$. Second, the onset temperature of the 20 nm Si/Fe$_2$O$_3$ (MM) is about 50 °C lower than that of the 100 nm Si/Fe$_2$O$_3$ (MM), confirming the importance of size effect. A smaller size NP has a larger specific surface area and a shorter diffusion distance for oxygen, and both factors contribute to the lower onset temperature. By contrast, the onset temperature of the 20 nm Si/Fe$_2$O$_3$ (CS) is about the same as that of the 100 nm Si/Fe$_2$O$_3$ (CS), indicating that intimate interfacial contact between Si and Fe$_2$O$_3$ in the CS structure has already effectively minimized the oxygen diffusion length. Hence, the initial size of the Si NP plays a negligible role here. In other words, the reaction onset temperature of Si/Fe$_2$O$_3$ nanothermites is mostly affected by their interfacial contact quality.
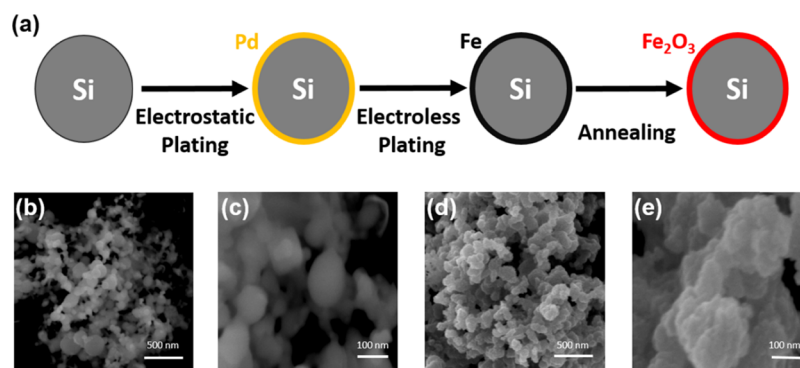

Figure 2. (a) Schematics of the electroless deposition process to coat Si NPs with Fe$_2$O$_3$ shells; SEM images of (b) initial Si NPs (100 nm); (c) magnification of (b); (d) Si/Fe$_2$O$_3$ CS NPs; and (e) magnification of (d).
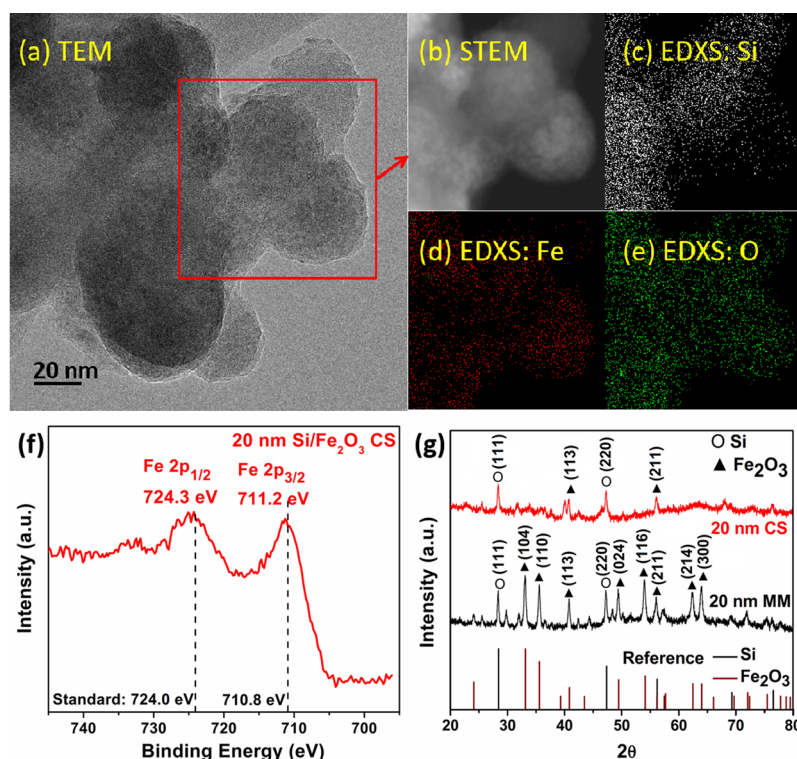
Figure 3. Material characterization of Si (20 nm)/Fe$_2$O$_3$ CS NPs: (a) TEM image; (b) STEM image of the boxed region in (a); EDXS mapping of (c) Si, (d) Fe, and (e) O elements in the boxed region in (a); (f) XPS spectra; and (g) XRD in comparison with that of Si/Fe$_2$O$_3$ MM NPs. These characterizations confirm the formation of Si/Fe$_2$O$_3$ CS NPs.
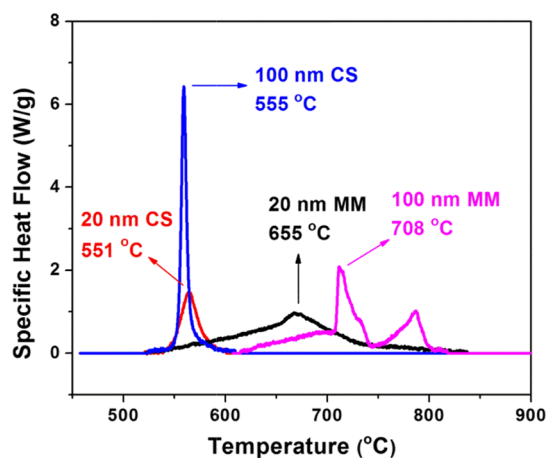

Figure 4. Baseline-corrected DSC traces of Si/Fe$_2$O$_3$ CS NPs and MM samples for two different initial sizes of Si particles (20 and 100 nm).

Finally, we compared the reaction onset temperatures of our Si/Fe$_2$O$_3$ CS NPs with those of Al/metal oxide nanothermites in the literature. We chose the Al/metal oxide nanothermites that have comparable Al size with our Si NPs for fair comparison, and the results are listed in Table 2. It is clear that Si/Fe$_2$O$_3$ CS NPs have comparable reaction onset temperatures as other Al/metal oxide nanothermites (460–580 °C). These data suggest that replacing Al with Si in thermites will have little change in terms of reaction onset temperatures.

CONCLUSIONS

We have shown that the easy surface functionality of Si allows a facile synthesis of Si/Fe$_2$O$_3$ CS NPs using a simple electroless plating method. The formed Si/Fe$_2$O$_3$ CS NPs have a reaction onset temperature of about 550 °C, which is about 100–150 °C lower than that of the MM samples. The lowering of the reaction onset temperature is caused by the enhanced intermolecular oxygen diffusion processes in the CS structure. In addition, the reaction onset temperature of the Si/Fe$_2$O$_3$ CS NPs is comparable to that of the commonly used Al-based nanothermites. Considering the easy surface functionalization property and comparable ignition properties, our study suggests that Si is another attractive fuel for thermites. Our synthesis methodology can be applied to form a diverse range of Si/metal oxide thermites for tailored applications.

METHODS

Synthesis of Si/Fe$_2$O$_3$ CS NPs. First, 100 mg of Si NPs was dispersed into 100 mL of isopropyl alcohol and sonicated for 15 min to break up the Si particle clusters. (3-Aminopropyl)-triethoxysilane (APTES, 1 mL, 99%, Sigma-Aldrich) and 0.5 mL of Milli-Q water were sequentially added to the Si NP solution and stirred at 70 °C for 1 h to functionalize the surface of Si with APTES. Second, the functionalized Si NPs were washed with deionized (DI) water and collected by centrifugation, and then, they were immersed in 40 mL of palladium chloride aqueous solution (20 mg of PdCl$_2$, Sigma-Aldrich, and 0.1 mL of reagent grade 37% HCl, Fisher Scientific) and stirred for 20 min. This electrostatic plating step coats the Si NPs with a thin layer of Pd film. Again, the Pd-coated Si NPs were washed with DI water and collected by centrifugation. The third step is to replace Pd with Fe by

Table 2. Comparison of Onset Temperatures of Different Thermites

sample	size of Si or Al (nm)	DSC heating rate (°C/min)	onset temperature (°C)	references
Si/Fe$_2$O$_3$ CS NPs	100	5	555	present work
Si/Fe$_2$O$_3$ CS NPs	100	10	551	present work
Si/Fe$_2$O$_3$ CS NPs	100	20	545	present work
Al/Fe$_2$O$_3$ xerogel nanocomposites	100	10	550	28
Al/Fe$_2$O$_3$ MM NPs	50	10	579	29
Al/Co$_3$O$_4$ nanocomposites	50	20	560	30
CuO/Al CS nanowires	100	5	549	9
Al/CuO MM NPs	80−150	10	460	31[a]
Al/Bi$_2$O$_3$ MM NPs	80−150	10	460	31[a]
Al/MoO$_3$ MM NPs	80−150	10	460	31[a]

[a]Might have used different definitions of onset temperature.

electroless plating. Specifically, the Pd-coated Si NPs were stirred for 5 min in 100 mL of DI water solution that contained 11.8 g of sodium citrate, 3.1 g of ammonium iron sulfate, 0.37 g of boric acid, 0.4 g of saccharin, and 0.1 g of lysine (all from Sigma-Aldrich). Then, 0.3 g of sodium borohydride (98%, Sigma-Aldrich) was added to the solution to initiate the electroless plating reaction. The resulted Si/Fe NPs were magnetic, so they were collected with a magnet. After rinsing with isopropyl alcohol and fully drying in vacuum, the Si/Fe NPs were annealed in a furnace in air at 450 °C for 5 h at a ramping time of 3 h. After annealing, the color of the NPs changed from black to red, indicating that the Fe shell was oxidized to Fe$_2$O$_3$.

DSC Measurement of Si/Fe$_2$O$_3$ CS and MM NPs. For a typical DSC measurement, a Si/Fe$_2$O$_3$ sample of about 5 mg (either CS or MM NPs) was placed in a 100 μL alumina crucible. The sample was heated in an inert argon environment (40 sccm) from room temperature to 900 °C at a heating rate of 5 °C/min. After the samples were cooled down to room temperature, they were heated with the same process again. The second-round heat flow traces were used to correct the baseline of the first-round heat flow traces following the method described previously.[25]

AUTHOR INFORMATION

Corresponding Author

*E-mail: xlzheng@stanford.edu. Phone: +1(650) 736-8953. Fax: +1(650) 723-1748 (X.Z.).

ORCID

Sidi Huang: 0000-0001-5703-0807
Sili Deng: 0000-0002-3421-7414
Jiheng Zhao: 0000-0001-8341-9031
Xiaolin Zheng: 0000-0002-8889-7873

Author Contributions

§S.H. and S.D. contributed equally to this work.

Notes

The authors declare no competing financial interest.

REFERENCES

(1) Wang, L. L.; Munir, Z. A.; Maximov, Y. M. Thermite Reactions: Their Utilization in the Synthesis and Processing of Materials. *J. Mater. Sci.* **1993**, *28*, 3693−3708.

(2) Orrù, R.; Sannia, M.; Cincotti, A.; Cao, G. Treatment and Recycling of Zinc Hydrometallurgical Wastes by Self-Propagating Reactions. *Chem. Eng. Sci.* **1999**, *54*, 3053−3061.

(3) Dreizin, E. L. Metal-Based Reactive Nanomaterials. *Prog. Energy Combust. Sci.* **2009**, *35*, 141−167.

(4) Gan, Y.; Qiao, L. Combustion Characteristics of Fuel Droplets with Addition of Nano and Micron-Sized Aluminum Particles. *Combust. Flame* **2011**, *158*, 354−368.

(5) Wang, J.; Qiao, Z.; Yang, Y.; Shen, J.; Long, Z.; Li, Z.; Cui, X.; Yang, G. Core−Shell Al-Polytetrafluoroethylene (PTFE) Configurations to Enhance Reaction Kinetics and Energy Performance for Nanoenergetic Materials. *Chem.—Eur. J.* **2016**, *22*, 279−284.

(6) Zhou, X.; Xu, D.; Yang, G.; Zhang, Q.; Shen, J.; Lu, J.; Zhang, K. Highly Exothermic and Superhydrophobic Mg/Fluorocarbon Core/Shell Nanoenergetic Arrays. *ACS Appl. Mater. Interfaces* **2014**, *6*, 10497−10505.

(7) Zhang, T.; Ma, Z.; Li, G.; Wang, Z.; Zhao, B.; Luo, Y. Electrostatic Interactions for Directed Assembly of High Performance Nanostructured Energetic Materials of Al/Fe$_2$O$_3$/Multi-Walled Carbon Nanotube (MWCNT). *J. Solid State Chem.* **2016**, *237*, 394−403.

(8) Séverac, F.; Alphonse, P.; Estève, A.; Bancaud, A.; Rossi, C. High-Energy Al/CuO Nanocomposites Obtained by DNA-Directed Assembly. *Adv. Funct. Mater.* **2012**, *22*, 323−329.

(9) Ohkura, Y.; Liu, S.-Y.; Rao, P. M.; Zheng, X. Synthesis and Ignition of Energetic CuO/Al Core/Shell Nanowires. *Proc. Combust. Inst.* **2011**, *33*, 1909−1915.

(10) Fischer, S.; Grubelich, M. *A Survey of Combustible Metals, Thermites, and Intermetallics for Pyrotechnic Applications*, 1996.

(11) Lafontaine, E.; Comet, M. *Nanothermites*; John Wiley & Sons, Inc.: Hoboken, NJ, USA, 2016.

(12) Thiruvengadathan, R.; Belarde, G. M.; Bezmelnitsyn, A.; Shub, M.; Balas-Hummers, W.; Gangopadhyay, K.; Gangopadhyay, S. Combustion Characteristics of Silicon-Based Nanoenergetic Formulations with Reduced Electrostatic Discharge Sensitivity. *Propellants, Explos., Pyrotech.* **2012**, *37*, 359−372.

(13) Yetter, R. A.; Risha, G. A.; Son, S. F. Metal Particle Combustion and Nanotechnology. *Proc. Combust. Inst.* **2009**, *32*, 1819−1838.

(14) Comet, M.; Siegert, B.; Schnell, F.; Pichot, V.; Ciszek, F.; Spitzer, D. Phosphorus-Based Nanothermites: A New Generation of Pyrotechnics Illustrated by the Example of n-CuO/Red P Mixtures. *Propellants, Explos., Pyrotech.* **2010**, *35*, 220−225.

(15) Comet, M.; Schnell, F.; Pichot, V.; Mory, J.; Risse, B.; Spitzer, D. Boron as Fuel for Ceramic Thermites. *Energy Fuels* **2014**, *28*, 4139−4148.

(16) Sullivan, K.; Young, G.; Zachariah, M. R. Enhanced Reactivity of Nano-B/Al/CuO MIC's. *Combust. Flame* **2009**, *156*, 302−309.

(17) Morita, M.; Ohmi, T.; Hasegawa, E.; Kawakami, M.; Ohwada, M. Growth of Native Oxide on a Silicon Surface. *J. Appl. Phys.* **1990**, *68*, 1272−1281.

(18) Terry, B. C.; Lin, Y.-C.; Manukyan, K. V.; Mukasyan, A. S.; Son, S. F.; Groven, L. J. The Effect of Silicon Powder Characteristics on the Combustion of Silicon/Teflon/Viton Nanoenergetics. *Propellants, Explos., Pyrotech.* **2014**, *39*, 337−347.

(19) Ledesma, H. A.; Tian, B. Nanoscale Silicon for Subcellular Biointerfaces. *J. Mater. Chem. B* **2017**, *5*, 4276−4289.

(20) Mason, B. A.; Groven, L. J.; Son, S. F.; Yetter, R. A. Combustion Performance of Several Nanosilicon-Based Nanoenergetics. *J. Propul. Power* **2013**, *29*, 1435−1444.

(21) Zhou, X.; Torabi, M.; Lu, J.; Shen, R.; Zhang, K. Nanostructured Energetic Composites: Synthesis, Ignition/Combustion Modeling, and Applications. *ACS Appl. Mater. Interfaces* **2014**, *6*, 3058−3074.

(22) Rossi, C.; Zhang, K.; Esteve, D.; Alphonse, P.; Tailhades, P.; Vahlas, C. Nanoenergetic Materials for MEMS: A Review. *J. Microelectromech. Syst.* **2007**, *16*, 919−931.

(23) Shimojo, F.; Nakano, A.; Kalia, R. K.; Vashishta, P. Electronic Processes in Fast Thermite Chemical Reactions: A First-Principles Molecular Dynamics Study. *Phys. Rev. E: Stat., Nonlinear, Soft Matter Phys.* **2008**, *77*, 066103.

(24) Mallory, G. O.; Hajdu, J. B. *Electroless Plating: Fundamentals and Applications*; William Andrew, 1990.

(25) Parimi, V. S.; Huang, S.; Zheng, X. Enhancing Ignition and Combustion of Micron-Sized Aluminum by Adding Porous Silicon. *Proc. Combust. Inst.* **2017**, *36*, 2317−2324.

(26) Silicon (Si) Nanopowder/Nanoparticles (Si, 98+%, 20−30 nm, Laser Synthesized, Polycrystalline Structure). http://www.us-nano.com/inc/sdetail/374 (accessed Jun 28, 2017).

(27) Nanomaterials, S. Nano Powder, Copper Nanoparticles, Lanthanum Oxide, Nano Powders, Titanium Nanoparticles. http://ssnano.com/inc/sdetail/silicon-nanoparticles-99--100-nm/147/291 (accessed Jun 28, 2017).

(28) Shin, M.-S.; Kim, J.-K.; Kim, J.-W.; Moraes, C. A. M.; Kim, H.-S.; Koo, K.-K. Reaction Characteristics of Al/Fe_2O_3 Nanocomposites. *J. Ind. Eng. Chem.* **2012**, *18*, 1768−1773.

(29) Zhao, N.; He, C.; Liu, J.; Gong, H.; An, T.; Xu, H.; Zhao, F.; Hu, R.; Ma, H.; Zhang, J. Dependence of Catalytic Properties of Al/Fe_2O_3 Thermites on Morphology of Fe_2O_3 Particles in Combustion Reactions. *J. Solid State Chem.* **2014**, *219*, 67−73.

(30) Zhang, D.; Xiang, Q. Electrophoretic Fabrication of an Al−Co_3O_4 Reactive Nanocomposite Coating and Its Application in a Microignitor. *Ind. Eng. Chem. Res.* **2016**, *55*, 8243−8247.

(31) Glavier, L.; Taton, G.; Ducéré, J.-M.; Baijot, V.; Pinon, S.; Calais, T.; Estève, A.; Rouhani, M. D.; Rossi, C. Nanoenergetics as Pressure Generator for Nontoxic Impact Primers: Comparison of Al/Bi2O3, Al/CuO, Al/MoO3 Nanothermites and Al/PTFE. *Combust. Flame* **2015**, *162*, 1813−1820.